Water Research 221 (2022) 118838

Contents lists available at ScienceDirect

Water Research

journal homepage: www.elsevier.com/locate/watres

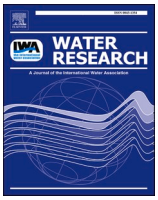

Bioavailable actinide fluxes to the Irish Sea from Sellafield-labelled sediments

Joshua D. Chaplin [a,*], Marcus Christl [b], Andrew B. Cundy [c], Phillip E. Warwick [c], David G. Reading [c], François Bochud [a], Pascal Froidevaux [a,*]

[a] Institute of Radiation Physics, Lausanne University Hospital and University of Lausanne, 1 Rue du Grand-Pré, Lausanne 1007, Switzerland
[b] Laboratory of Ion Beam Physics, ETH Zürich, Otto-Stern-Weg, Zürich 8093, Switzerland
[c] School of Ocean and Earth Science, National Oceanography Centre, University of Southampton, European Way, Southampton SO14 3ZH, UK

A B S T R A C T

Nuclear discharges to the oceans have given rise to significant accumulations of radionuclides in sediments which can later remobilise back into the water column. A continuing supply of radionuclides to aquatic organisms and the human food chain can therefore exist, despite the absence of ongoing nuclear discharges. Radionuclide remobilisation from sediment is consequently a critical component of the modelled radiation dose to the public. However, radionuclide remobilisation fluxes from contaminated marine sediments have never been quantitatively determined *in-situ* to provide a valid assessment of the issue. Here, we combine recent advances in the Diffusive Gradients in Thin Films (DGT) sampling technique with ultrasensitive measurement by accelerator mass spectrometry (AMS) to calculate the remobilisation fluxes of plutonium, americium and uranium isotopes from the Esk Estuary sediments (UK), which have accumulated historic discharges from the Sellafield nuclear reprocessing facility. Isotopic evidence indicates the local biota are accumulating remobilised plutonium and demonstrates the DGT technique as a valid bioavailability proxy, which more accurately reflects the elemental fractionation of the actinides in the biota than traditional bulk water sampling. These results provide a fundamental evaluation of the re-incorporation of bioavailable actinides into the biosphere from sediment reservoirs. We therefore anticipate this work will provide a tool and point of reference to improve radiation dose modelling and contribute insight for other environmental projects, such as the near-surface and deep disposal of nuclear waste.

1. Introduction

Nuclear activities have routinely released radionuclides to the oceans which accumulate within marine organisms. This presents a radiotoxicity and biotoxicity hazard to a range of biota, including human consumers. Radionuclides in the seawater, depending on their speciation and particle reactivity, can also accumulate over time in sediment bodies *via* adsorption and other removal processes. Significant radionuclide accumulations have contaminated sediments near to sites of authorised or accidental nuclear discharges, including Fukushima (Japan) (Mouri et al., 2014; Taniguchi et al., 2019; Takata et al., 2015), La Hague (France) (Cundy et al., 2002) and Sellafield (UK) (Morris et al., 2000; McDonald et al., 2001; Hunt et al., 2013). Such accumulation may be reversible over longer time periods however, and sediment-associated radionuclides have been observed to remobilise back into the surrounding water in various settings (Morris et al., 2000; Hunt et al., 2013; Mitchell et al., 2001; Caborn et al., 2016). Several mechanisms have been proposed for this, including chemical mobilisation processes and bioturbation (Kershaw et al., 1983). Therefore, a reduction or cessation in nuclear discharges does not guarantee the removal of a significant supply of radionuclides to local waters, where they can again become available for uptake by biota. This effect has been observed near to the UK's Sellafield facility for example, where plutonium concentrations in seaweed and shellfish changed very little in the years following a very steep reduction in nuclear discharges to the Irish Sea (Ryan et al., 1999). Radiation dose modelling must therefore account for radionuclide remobilisation in order to be fully comprehensive. This is critical around sites such as Sellafield, where the sediments of the Cumbrian coastal region contain significant radionuclide loadings (>20 Bq g^{-1} for some actinides). This presents long-term radiological risk implications, including from the in-growth of ^{241}Am from accumulated ^{241}Pu (Day and Cross, 1981).

Despite this, no time-integrated and *in-situ* method currently exists which can determine the remobilisation fluxes of actinides from marine sediments. The need for such a technique is highlighted by large temporal and spatial inconsistencies in sediment-water partition coefficients (k_d) for radionuclides (Agency, 2004). These k_d values have been used to indicate radionuclide remobilisation in the Cumbrian coastal region

* Corresponding authors.
E-mail addresses: joshua.chaplin@chuv.ch (J.D. Chaplin), pascal.froidevaux@chuv.ch (P. Froidevaux).

https://doi.org/10.1016/j.watres.2022.118838
Received 21 April 2022; Received in revised form 22 June 2022; Accepted 7 July 2022
Available online 8 July 2022

(Hunt et al., 2013; Mitchell et al., 2001) alongside *ex-situ* partitioning and desorption experiments (Takata et al., 2015), but cannot validly replicate *in-situ* geochemical conditions and their variability.

The Diffusive Gradients in Thin Films (DGT) technique is a well-established passive sampling method and bioavailability proxy which has previously been employed to calculate remobilisation fluxes for various metals from sediment (Harper et al., 1998; Wu et al., 2015; Norgbey et al., 2020; Zhang et al., 1995; Gao et al., 2016; Zhang et al., 2001). When deployed in sediments, DGT samplers function as a sink for their target analyte(s), mimicking the dynamic action of a plant root as they induce a flux of labile (bioavailable) species *in-situ* from porewater to their resin-gel (Zhang et al., 2001; Davison, 2016). Recently developed resin-gels (Chaplin et al., 2021, 2022) have made possible the measurement of actinides in the marine environment by DGT. In this work, we combined deployments of DGT samplers with ultrasensitive measurement by accelerator mass spectrometry (AMS) (Christl et al., 2013), to calculate remobilisation fluxes of plutonium, americium and uranium isotopes from the Esk Estuary sediments (UK) to the Irish sea (Fig. 1). Isotopes ($^{239\text{-}241}$Pu, ^{241}Am and ^{236}U) captured by the DGT samplers and in local biota and seawater were measured at the compact, actinide-optimised ETH-Zürich AMS facility TANDY (Christl et al., 2013), allowing for the detection of isotopes at the sub-femtogram level. Analysis of isotopic signatures throughout the DGT-sampled sediment profiles (Figs. 2 and 3), local biota (Fig. 3) and seawater (Fig. 3) allowed us to constrain the origins of the contamination throughout the Esk Estuary and assess the ability and validity of the DGT technique as a proxy for actinide bioavailability determination.

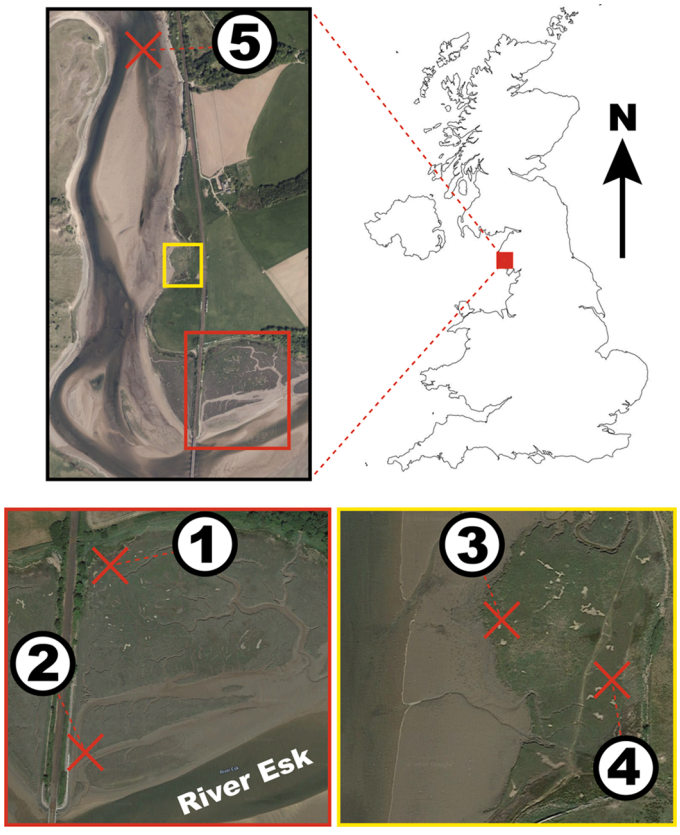

Fig. 1. Sampling sites. Sites 1–5 (red crosses) in the Esk Estuary, UK. See Methods Table 1 for coordinates and elevation.

2. Materials and methods

2.1. Site selection

We selected the Ravenglass Estuary for the deployment of DGT samplers due to its well documented and significant sedimentary inventory of legacy Sellafield-derived actinides. Two sampling campaigns were undertaken. Campaign one was undertaken between 24th August 2020 and 7th September 2020, and campaign two was undertaken between 24th May 2021 and 7th June 2021. During campaign one, DGT Research® R-SP sediment probe housings containing the IIP-Y^{3+} and KMS-1 configurations (Chaplin et al., 2021) were deployed, at sites 1–4 (Methods Fig. 1, Ordnance Survey (OS) grid references and elevations are given in Methods Table 1). During campaign two, custom in-house "DGT-55" sediment probe housings containing the IIP-Y^{3+} and KMS-1 configurations were deployed at sites 1 and 5, sampling deeper up to 55 cm depth. Sites 1-4 are ungrazed marshland, with gradation shown between the lower to upper marsh environments from the River Esk main channel. The Upper Railway Marsh (site 1) is a mixed high marsh sward with sea aster, sea arrow grass, sea rush (*Juncos maritimus*), salicornia (*Salicornia europaea*), sea plantain and sea purslane (*Sesuvium portulacastrum*). The Lower Railway Marsh (site 2) is characterised by sea aster (*Tripolium pannonicum*), sea plantain (*Plantago maritima*) and sea arrowgrass (*Triglochin maritima*). The Brighouse Marsh (Upper - site 3, and Lower – site 4) is a consistent mixed high marsh sward including sea aster, sea lavender (*Limonium vulgare*) and sea plantain in the upper region, with additional sea purslane and sea aster more common in the lower region. Site 5 is an intertidal sandflat near to the mouth of the Esk Estuary which exposes a lagoon at low spring tide.

2.2. DGT sampler manufacture

Diffusive gels were purchased from DGT Research® (Lancaster, UK). The KMS-1 resin was synthesised according to the hydrothermal method reported in point C of the Supporting Information of Manos et al. (2008) IIP-Y^{3+} was synthesised in a modified procedure, following that of Chauvin et al. (2006) but with the ligand L_1 instead synthesised according to Scheme 1 of Chaplin et al. (2021) The KMS-1 and IIP-Y^{3+} DGT resin-gels were synthesised as described by Chaplin et al. (2021) The internal resin distribution in the synthesised resin-gel was verified to be homogenous before being assembled into the DGT sampler housing. DGT R-SP sediment probe housings were purchased from DGT Research Ltd (Lancaster, UK) and used to house the KMS-1 and IIP-Y^{3+} configurations during the first sampling campaign. Our custom DGT-55 sediment probes were designed and manufactured in the workshop of Lausanne University Hospital's Institute of Radiation Physics (CHUV-IRA) and were used to house the KMS-1 and IIP-Y^{3+} configurations during campaign two. 105 cm^2 surface area DGT samplers as described by Cusnir et al. (2015) were also used to house KMS-1 and IIP-Y^{3+} sampling configurations for seawater deployments. These were encased

Table 1
Details of sampling sites used for DGT sediment probe deployments during campaigns one and two.

Site	Location	Setting	OS Grid Reference	Elevation ASL
1	Railway Marsh	Upper marsh, intertidal	08818 94573, ± 4 m	4 m
2	Railway Marsh	Lower marsh, intertidal	08847 94786, ± 9 m	5 m
3	Brighouse Marsh	Upper marsh, intertidal	08716 95087, ± 4 m	2 m
4	Brighouse Marsh	Lower marsh, intertidal	08756 95080, ± 8 m	5 m
5	Ravenglass Channel	Marine, intertidal	08636 95776, ± 8 m	2 m

in protective stainless-steel holders and deployed facing upwards at roughly a 45° angle, secured to poles in the seabed. Prior to sampling, DGT samplers were stored and transported in sealed plastic bags with several drops of 0.3 M NaCl inside the bags to maintain moisture for a total period of no more than 3 weeks.

2.3. DGT and porewater peeper sampling

DGT samplers were unsealed from their packaging in the field. Care was taken not to step within at least 50 cm of the point of insertion into the sediment, allowing the natural sediment porosity and pre-existing porewater pathways to remain undisturbed. During campaign one, DGT Research® (Lancaster, UK) R-SP sediment probes were deployed into sediment at least 30 cm apart from each other. During campaign two, custom in-house DGT-55 sediment probes were inserted into sediment at least 30 cm apart from each other and at least 2 m from the exact deployment site of the samplers during campaign one. 55 cm long porewater peepers, with 20 mL compartments at 2.5 cm intervals and sealed with 0.45 μm polyethersulphone filter membrane, were deployed adjacent to DGT samplers during campaign two. This allowed for the porewater concentration to be determined by diffusion at equilibrium *in-situ*, which is particularly important for accurate readings of U (Toole et al., 1984). All DGT samplers and porewater peepers were left *in-situ* for 14 days during both campaigns. This depleted the analyte from the porewater, inducing the desorption of labile sediment-adsorbed species into the porewater to maintain the equilibrium defined by the k_d. An extended deployment period (> 1–3 days) in sediment therefore ensures the flux of the analyte to the DGT sampler is exclusively diffusion-controlled by depletion from the sediment. Additionally, this minimises the impact caused by the initial disturbance of inserting the sampler by allowing the sediment profile to re-establish *via* redox buffering mechanisms (Davison, 2016).

2.4. Sediment core sampling

Sediment cores were extracted at the same time as the DGT Research® R-SP DGT sediment probe deployments on 24th August 2020, by hammering a length of PVC pipe into the marshland around 50 cm from the DGT samplers at each site. Cores were sectioned into slices of around 2 cm thickness, freeze-dried, ground, and the powder was measured in HPGe gamma spectrometers to obtain ^{137}Cs and ^{241}Am bulk concentration data. Suitable aliquots (5–300 mg) of the powdered core fractions were then immersed in 20 mL of concentrated HNO_3 and dispersed using ultrasound. After at least 24 h of leaching at a temperature close to reflux, the powder was filtered using a 0.45 μM syringe filter and prepared for Pu separations (as described in the following sections) to determine the $^{239+240}$Pu bulk concentrations by alpha spectrometry, using 450 mm^2 passivated implanted planar silicon detectors and Alpha-Analyst (Canberra, France) software.

2.5. Sediment core age model

Sediment cores were dated according to the depth of the activity concentration maxima of ^{137}Cs, $^{239+240}$Pu and ^{241}Am in the core profile. The years of maximum discharge from the Sellafield facility were 1975 for ^{137}Cs, 1973 for $^{239+240}$Pu and 1974 for ^{241}Am (retrieved from Gray et al. 1995). The surface of the sediment core was considered as the date of retrieval (24 August 2020). The depth of the maximum activity concentration of the radioanalyte was considered as 01 January for the year of maximum discharge from Sellafield. A lag/ transit time of 1-3 months has previously been observed between the discharge of some radionuclides (^{106}Ru, ^{144}Ce, ^{95}Zr and ^{95}Nb) from Sellafield and their deposition in Esk Estuary sediments (Hetherington and Jefferies, 1974). This was therefore considered negligible at the resolution of our core profiles and not included in the model calculations.

The sediment accumulation rates (cm.yr^{-1}) based on ^{137}Cs, $^{239+240}$Pu and ^{241}Am were calculated by dividing the distance between the surface and the depth of maximum activity concentration by the amount of time between the retrieval date and the year of maximum discharge, assuming a constant rate of deposition (Methods Table 2). The final accumulation rate of each core was calculated as the average of the three accumulation rates calculated for ^{137}Cs, $^{239+240}$Pu and ^{241}Am. This model produced an accumulation rate of 0.605 cm.yr^{-1} at site 1 (which is consistent with previous work at this marsh (Morris et al., 2000; Oh et al., 2009; Marsdem et al., 2006)), 0.336 cm.yr^{-1} at site 3 and 0.308 cm.yr^{-1} at site 4. The activity concentration maxima were not necessarily observed at the lower reach of the core retrieved at site 2, so this profile could not be objectively dated.

2.6. Biota sampling

Samples of marsh vegetation, seaweed and periwinkles were retrieved on 7th September 2020 between sites 1–5. 'Marsh vegatation' includes sea purslane (*Sesuvium porulacastrum*), salicornia (*Salicornia Europea*) and sea plantain (*Plantago maritima*). The common periwinkle (*Littorina littorae*) was the only live mollusc species found on site, and two different species of seaweed were collected: common bladderwrack (*Fucus vesiculosis*) and Irish moss (*Chondrus crispus*). All marsh vegetation and seaweed samples were retrieved whole from the root, except for separate additional samples of the endmost ≤2.5 cm of *Fucus vesiculosis* fronds, at the furthest point from the root. Samples were collected and stored in sealed airtight plastic bags and frozen in a cooler on site prior to transportation to the laboratory.

2.7. Radiochemical procedures: DGT resin-gels

DGT sampler housings were disassembled, and the filter membranes and diffusive gels were discarded. The resin-gel in DGT Research R-SP sediment probes was cut into 5 cm x 1.8 cm or 3 cm x 1.8 cm sections using a scalpel. 5×4 cm resin-gels in DGT-55 sediment probes were retrieved whole. Resin-gels or resin-gel segments were gently washed with a stream of deionised water and placed in a new glass beaker which was pre-washed with 0.1M HCl. 10 mL of 8 M HNO_3 plus five drops of H_2O_2 were added to elute Pu and U from the KMS-1 resin-gels, and 10 mL of 3 M HCl was added to elute Am from IIP-Y^{3+} resin-gels. Appropriate tracers were added to the eluent at this point; around 1 pg each of ^{233}U and ^{242}Pu for KMS-1 resin-gel samples and ^{243}Am for IIP-Y^{3+} resin-gel samples. Resin-gels were left in the eluent overnight and separated into a clean beaker using a 0.45 μM syringe filter, with three deionised water beaker washouts of approximately 5 mL also passed through the syringe filter. All filtered eluents were evaporated to dryness (the 'sample residue'). The sample residue was then put through radiochemical separations (see the 'Plutonium separations' section next for KMS-1 resin gel samples, or the 'Americium separations' section next for IIP-Y^{3+} resin gel samples).

Table 2
Sediment profile accumulation rates.

Site	Radioanalyte	Accumulation rate (cm. yr^{-1})	Average accumulation rate (cm.yr^{-1})
1	^{137}Cs	0.592	0.605
	$^{239+240}$Pu	0.573	
	^{241}Am	0.650	
2	^{137}Cs	Activity concentration maxima not observed in core profile	
	$^{239+240}$Pu		
	^{241}Am		
3	^{137}Cs	0.329	0.336
	$^{239+240}$Pu	0.344	
	^{241}Am	0.336	
4	^{137}Cs	0.301	0.308
	$^{239+240}$Pu	0.315	
	^{241}Am	0.308	

2.8. Radiochemical procedures: biota samples

Marsh vegetation and seaweed samples were washed thoroughly with deionised water. Externally precipitated actinides were then eluted from the exterior of the leaves by immersing marsh vegetation and seaweed in 1 L 0.1 M citric acid / 0.1 M sodium citrate buffer for one hour. This solution was then decanted, and the plants were thoroughly rinsed with deionised water before desiccation at 80°C for 24 hours and then calcination overnight at 550°C. Ashes were dissolved in 20 ml concentrated HNO_3 in Teflon® canisters, traced with ~1 pg ^{233}U, ^{242}Pu and ^{243}Am each, and wet ashed in a pressurised microwave reactor (Milestone UltraClave IV) at 180°C under 50 bars pressure. The sample was decanted and evaporated to dryness (the 'sample residue'). The sample residue was prepared for sequential extraction of Pu, then U, then Am (see following sections).

2.9. Plutonium separations

Pu separations were always performed prior to U separations, as described by Chaplin et al. (2021) for sequential Pu and U extraction from KMS-1 resin-gel samples. The sample residue was redissolved in 10 mL 8 M HNO_3. 50 µg Fe(III) dissolved in 1 mL 0.1 M HCl was added, and the sample was gently agitated. 1 mL 100 mg.ml^{-1} ascorbic acid solution was added to reduce all Fe(III) to Fe(II), consequently co-reducing all Pu in the sample to Pu(III). 40–60 mg $NaNO_2$ was added, and the sample was heated on a hot plate at 150 °C for 10 min to fix all Pu in the sample to Pu(IV). The sample was allowed to cool, and Pu(IV) was extracted on a Bio-Rad Poly-Prep column containing 2 mL of Bio-Rad AG 1-X4 resin, preconditioned with 10 mL 8 M HNO_3. The column was washed with 3×5 mL 8M HNO_3 beaker washouts and subsequently with 15 mL of 9 M HCl to elute any Th present in the sample. The waste fraction was retained for subsequent separation of U (and then Am, for biota samples). Pu was eluted from the column with 15 mL of $H_3NO{\cdot}HCl$ (5% aq.). $H_3NO{\cdot}HCl$ in the eluate was destroyed in an acid fume cupboard by dropwise addition of HNO_3 (concentrated) and the remaining eluate solution was evaporated gently at 150 °C. The eluate residue was prepared for AMS target manufacture (see 'AMS target preparation' section).

2.10. Uranium separations

The waste fraction from Pu separations was evaporated to dryness and redissolved in 3 mL of 8 M HNO_3. 100 mg of UTEVA (Triskem, France) resin was packed into a 1 mL micropipette cartridge column and conditioned with 3×1.5 mL 8 M HNO_3. The samples were passed though the column and 3×1.5 mL 8 M HNO_3 beaker washouts were then transferred through the column. The columns were further washed with 3×1.5 mL 6 M HCl to remove residual Th, and U was eluted with 10 mL of 0.01M HCl. The waste fraction of biota samples was retained for subsequent separation of Am. The eluate was evaporated gently at 150°C and prepared for AMS target manufacture (see 'AMS target preparation' section).

2.11. Americium separations

The sample residue was redissolved in deionised water at pH 3.0 ± 0.1 (adjusted to pH 3.0 ± 0.1 with dropwise addition of 0.1 M HCl). A 2 mL cartridge was packed with IIP-Y^{3+} resin (Chaplin et al., 2021; Chauvin et al., 2006) and pre-washed with 5 mL 0.1 M $C_2H_2O_4$. The cartridge was then conditioned with 20 mL of deionised H_2O (pH 3.0 ± 0.1). The loading solution was collected into a syringe and passed through the cartridge using a syringe pusher at 1 mL.min^{-1}. The column was washed with 3 × 5 mL H_2O (pH 3.0 ± 0.1) beaker washouts and Am (III) was eluted with 20 mL of 3 M HCl. The eluate was evaporated gently at 150°C and prepared for AMS target manufacture (see 'AMS target preparation' section).

2.12. AMS target preparation and measure

Residues of the evaporated eluates were dissolved in 10 ml 0.1 M HCl. The sample was heated gently at 50°C and stirred at 150 rpm. 1 ml Fe(III) 2 mg.ml^{-1} solution was added and left to equilibrate in the stirred solution for at least 15 minutes. Fe-hydroxides were then precipitated at pH 7 by dropwise addition of NH_4OH (30%) and left to equilibrate in the stirred solution for at least 15 minutes. The actinides in the sample were co-precipitated with the Fe-hydroxides. The precipitate was decanted and centrifuged, then re-suspended in Milli-Q water and re-centrifuged to wash out any remaining NH_3 prior to baking. The precipitate was transferred into a 2.5 mL quartz crucible (held within an open-top brass sample wheel to withstand high heating) and desiccated at 80°C until dry. The powder was baked at 650°C for at least 4 hours to convert Fe into the oxide form. 2–3 mg Nb powder was added to the baked sample powder and mixed with a spattle. The powder was then compressed into a modified NEC cathode as per ETH Zürich's Laboratory of Ion Beam Physics (ETHZ-LIP)'s internal procedure (Christl et al., 2013). U measurements were normalised to the ETHZ-LIP in-house ZUTRI standard (Christl et al., 2013) and Pu measurements were normalised to the ETHZ-LIP in-house CNA standard (Christl et al., 2013). Am measurements were normalised to a standard produced from certified NIST-traceable ^{241}Am and ^{243}Am sources provided by the Radiometrology group of CHUV-IRA. Most measurements were performed using EHTZ-LIP's TANDY cAMS system (Christl et al., 2013), with some U measurements performed on the recently developed MILEA system. For note, if a U target was planned for measure by MILEA, it was co-precipitated with 1.25 ml Fe(III) 2mg.ml^{-1} solution and mixed with 6 mg of Nb.

2.13. Radioactive decay corrections

^{241}Pu ($t_{1/2}$ = 14.4 years) masses were decay-corrected from the date of measurement to the reference date of sampling (or the midpoint of 14-day DGT sampler deployments). In all samples except IIP-Y^{3+} DGT samplers for Am measure (which do not capture Pu), the consequent ingrowth of ^{241}Am from the decay of measured ^{241}Pu present in the same sample was also accounted for. Other measured isotopes (^{236}U, ^{239}Pu, ^{240}Pu, ^{241}Am) have much longer half-lives and decay correction was therefore not performed as it does not significantly alter the results.

2.14. Calculation of c_{DGT}

The average analyte concentration at the sediment-porewater interface according to the DGT sampler, c_{DGT} (g.mL^{-1}), was calculated using Eq. (1):

$$c_{DGT} = \frac{A \cdot \Delta g}{D \cdot t \cdot S} \quad (1)$$

A is the quantity of the analyte eluted from the resin-gel (in this work calculated by AMS, with the atom ratio of the analyte isotope to the tracer isotope measured and then converted to g); t is the exposition time (seconds); S is the surface area (cm^2) of the sampler section exposed to the sediment; Δg is the thickness (cm) of the material diffusion layer, and D is the diffusion coefficient of the analyte (cm^2.s^{-1}). D was taken from the values reported for U, Pu and Am in seawater in Table 1 of Chaplin et al. (2021) and calibrated to the average seawater temperature during the deployment period (Methods Table 3) using the Stokes-Einstein correction (Eq. (4) of Chaplin et al. (2021)). Daily average seawater temperatures for Whitehaven harbour for each day of both sampling campaigns were retrieved from seatemperature.info on 16 June 2021. These were used to calculate the average temperature throughout the deployment period to calibrate D. We confirmed using porewater concentration (c_{pw}) data produced using adjacent peepers, that the rate of solute resupply (Davison, 2016) (R, = c_{DGT}/c_{pw}) was

<<0.1 (Supporting Information Table 2). This confirmed that the supply of the analyte to the DGT sampler was diffusion-controlled. The 14-day deployment period therefore completely depleted the sediment in the vicinity of the DGT sampler, to the point where supply to the DGT sampler was diffusion-controlled only. In this case, we normalised c_{DGT} to 24 h, as is appropriate to represent the solution concentration and the maximum induced flux to the resin-gel (Davison, 2016). The normalised c_{DGT} was used to calculate the remobilisation flux (F).

2.15. Calculation of the remobilisation flux

The remobilisation flux, F (fg.hr^{-1}.cm^{-2}) was calculated using Eq. (2):

$$F = \frac{D \cdot c_{DGT}}{\Delta g} \quad (2)$$

The D used in this work for sediment and seawater DGT deployments are presented in Methods Table 3, below.

In this work,

$$\Delta g = \delta^{g} + \delta^{f} + \delta^{dbl} \quad (3)$$

Where δ^{g} is the thickness of agarose cross-linked polyacrylamide (APA) diffusive gel used during deployments (0.078 cm or 0.039 cm), δ^{f} is the thickness of the membrane filter (0.014 cm), and δ^{dbl} is the diffusive boundary layer. For DGT samplers deployed in seawater, this was taken as 0.049 cm from Chaplin et al. (2021)). For DGT samplers deployed in sediment, $\delta^{dbl} = 0$ cm.

3. Results and discussion

3.1. Remobilisation flux variations and controls

Remobilisation fluxes of Pu, Am and U in the Esk Estuary significantly vary both temporally (Fig 1a,b) and spatially (Fig. 1a, f and b–e). This underlines the need for a time-integrated method for their valid determination. Pu and Am remobilisation fluxes between 24th May and 7th June 2021 were significantly higher in fine-grained sediment (silt and clay) of intertidal marshland (average $^{239+240+241}$Pu and ^{241}Am fluxes of 1.9 ± 0.5 and 0.120 ± 0.015 fg·h^{-1}·cm^{-2} , respectively, Fig. 1a) than in sand in the lower estuary channel (0.5 ± 0.03 and 0.010 ± 0.003 fg·h^{-1}·cm^{-2} , respectively, Fig. 1f). Higher fluxes may be expected for sandy sediments compared to equally contaminated silts and clays, if considering the main controlling factor is the lower k_d of sand versus k_d of silt and clay for Pu and Am. The results here therefore reflect that the finer sediments hold a larger actinide inventory than the coarser sand, and therefore supply more Pu and Am to the interstitial waters despite having a higher and therefore more retentive k_d.

There were consistent temporal variations in the Pu fluxes (measured by DGT samplers configured with the KMS-1 resin-gel) and the Am fluxes (measured by separate DGT samplers configured with the IIP-Y^{3+} resin-gel) between two deployment periods, nine months apart. At site 1, the $^{239+240+241}$Pu and ^{241}Am fluxes in the top 20 cm of sediment, respectively averaged 10 ± 2 and 1.09 ± 0.09 fg·h^{-1}·cm^{-2} between 24th August and 7th September 2020 (Fig. 1b), compared to 1.3 ± 0.5 and 0.150 ± 0.02 fg·h^{-1}·cm^{-2} between 24th May to 7th June 2021 (Fig. 1a). We additionally determined the flux of anthropogenic ^{236}U to the same KMS-1-configured DGT samplers that measured the Pu fluxes. We found the opposite trend with the ^{236}U fluxes compared to Pu and Am between the two sampling campaigns; the ^{236}U fluxes were lower in the top 20 cm of sediment at Site 1 between 24th August and 7th September 2020 (0.07 ± 0.005 fg·h^{-1}·cm^{-2}) than between 24th May to 7th June 2021 (0.116 ± 0.007 fg·h^{-1}·cm^{-2}). As U is a highly conservative radionuclide, compared to non-conservative Pu and highly non-conservative Am, this suggests that more infiltration of seawater into the marsh sediments during this period. Further evidence for this is provided by the lower average ^{240}Pu/^{239}Pu signatures of the DGT resin-gel segments deployed between 24th May to 7th June 2021 (0.197 ± 0.015, Fig. 2a) compared to those deployed between 24th August and 7th September 2020 (0.224 ± 0.018, Fig. 2b). This suggests a dilution of higher sediment ^{240}Pu/^{239}Pu signature (Figs. 2a–e, 3a) with the lower ^{240}Pu/^{239}Pu signature of the seawater, which is closer to global fallout (Fig. 3), Furthermore, the ^{236}U/^{239}Pu ratio also demonstrated this trend, indicating a much higher relative presence of ^{236}U between 24th May to 7th June 2021 (Fig. 2a, b). This points to the influence of the hydraulic regime as a driving factor behind the remobilisation fluxes at site 1. The organic content of the sediments also likely has an influence on the magnitude of the fluxes. A steep drop in the Pu fluxes at the 12.5 cm depth midpoint of Fig. 1a corresponds with a layer from an adjacent core retrieved during the same sampling period, which has decreased Si, K, Ca, Fe and Rb and increased S (Supporting Information Fig. 1, marked as (c_{org}). This indicates an organic-rich layer, as further evidenced by a lighter horizon on the X-radiograph. The association of Pu with organic humic and fulvic acids has previously been shown to decrease its diffusion coefficient (Cusnir et al., 2014), possibly explaining the drop observed in the fluxes in Fig. 1a. We consider other influences on the fluxes to be minimal; for example, the fluxes generally do not show major variations throughout the profiles and especially at depth, whilst factors such as potential aging effects may be expected increase the sediment-water k_d of metal cations and therefore significantly reduce the fluxes. Furthermore, previous work has demonstrated that U aged in soil *in-situ* for >2000 years behaves similarly to artificially introduced depleted U (Straub et al., 2022).

Table 3
Average seawater temperatures and corresponding D used to calculate c_{DGT}.

Campaign	Average seawater temperature (Whitehaven)	D (U)	D (Pu)	D (Am)
1 (24 Aug – 07 Sept 2020)	17.28°C	1.43×10^{-6} cm^2.s^{-1}	2.13×10^{-6} cm^2.s^{-1}	1.29×10^{-6} cm^2.s^{-1}
2 (24 May – 07 June 2021)	12.63°C	1.20×10^{-6} cm^2.s^{-1}	1.79×10^{-6} cm^2.s^{-1}	1.09×10^{-6} cm^2.s^{-1}

3.2. Constraining the actinide sources using isotopic reports

We analysed several isotopic fingerprints in the sediments (Figs. 2 and 3), seawater (Fig. 3) and local biota (Fig. 3) of the Esk Estuary. ^{240}Pu/^{239}Pu and ^{241}Pu/^{239}Pu atom ratios reflect the degree of Pu-burn up of the source material and therefore indicate its origin, whilst the ^{236}U/^{239}Pu and ^{241}Am/^{239}Pu atom ratios are moreover influenced by geochemical elemental fractionation. ^{240}Pu/^{239}Pu in the top 10 cm of the marsh sediments between Sites 1–4 averaged 0.215 ± 0.016 (n = 13; Figs. 2a–e, 3a). This is significantly higher than the seawater at site 5 (lower marine estuary, 0.196 ± 0.015 (n = 3)) and site 2 (middle estuary with strong mixing of seawater and freshwater, 0.191 ± 0.015 (n = 3)). The seawater and adjacent seawater DGT probes correspond closer to the global fallout value of 0.18 ± 0.01 (Fig. 3a). These values fall significantly below the IAEA-381 reference Irish Seawater from 1993, which more closely matches the signature of the sediments (0.23 ± 0.02) (Corcho Alvarado et al., 2022). Additionally, this is higher than the IAEA-135 Irish Sea sediment reference material from 1992 (0.205 ± 0.002) (Corcho Alvarado et al., 2022). This indicates that the marsh sediments have accumulated more Pu from reprocessing discharges (which has a higher signature than that of global fallout) from the seawater over the preceding decades. Additionally, modern Irish Seawater has become diluted with the residual global fallout

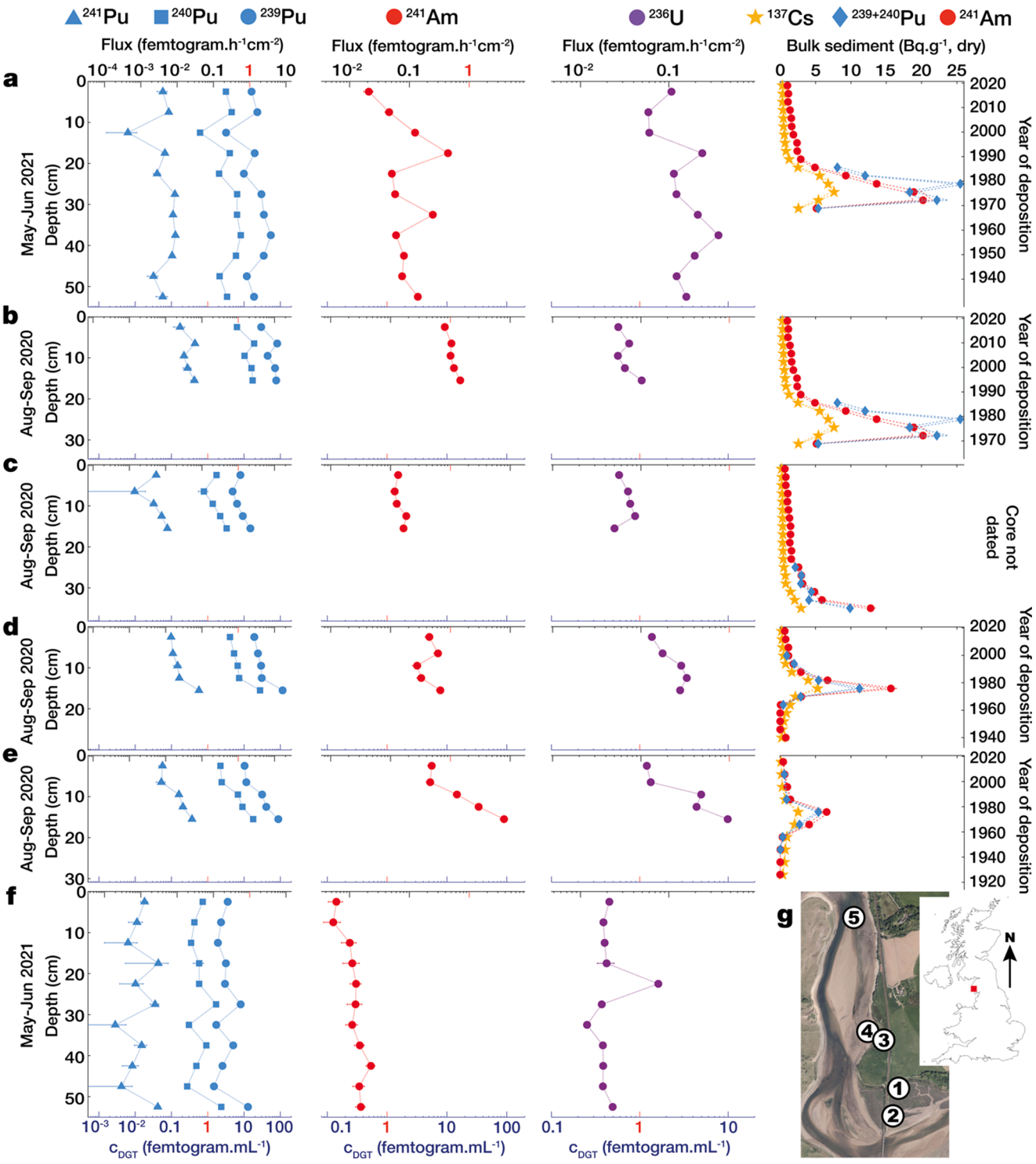

Fig. 1a. Remobilisation fluxes, c_{DGT} and bulk sediment inventory at Sites 1-5 in the Esk Estuary. $^{239\text{-}241}$Pu, ^{241}Am and ^{236}U remobilisation fluxes and c_{DGT}, and ^{241}Am, $^{239+240}$Pu, and ^{137}Cs bulk sediment concentrations at (**a**) Site 1, 24th May - 7th June 2021 (exception: bulk core data from a core retrieved on 24th August 2020); (b) Site 1, 24th August - 7th September 2020; (c) Site 2, 24th August - 7th September 2020; (d) Site 3, 24th August - 7th September 2020; (**e**) Site 4, 24th August - 7th September 2020; (**f**) Site 5, 24th May - 7th June 2021 (no sediment core retrieved due to heavily mixed sand). (**g**) Sampling sites 1–5 in the Esk Estuary (see Methods Fig. 1). Data aligned to c_{DGT} (bottom axis). ±2σ uncertainties.

^{240}Pu/^{239}Pu signature since the cessation of the Sellafield discharges.

The bulk sediment profiles in the sediment cores at Sites 1–4 demonstrate co-incident maxima in the $^{239+240}$Pu, ^{241}Am, and ^{137}Cs profiles with depth (Fig. 2a–e), representing accumulation with sedimentation over time as a function of the seawater concentration. With ^{210}Pb-dating problematic around the Cumbrian coastline due to other non-nuclear anthropogenic discharges (McCartney et al., 1990), we used the $^{239+240}$Pu, ^{241}Am and ^{137}Cs maxima to date the cores (see Methods for age model). The presence of well-defined subsurface activity maxima in bulk sediment, which can be correlated with the Sellafield discharge history, shows a lack of large-scale mixing or bioturbation in these marsh sediments. The period from the 1950s to early 1960s (when the

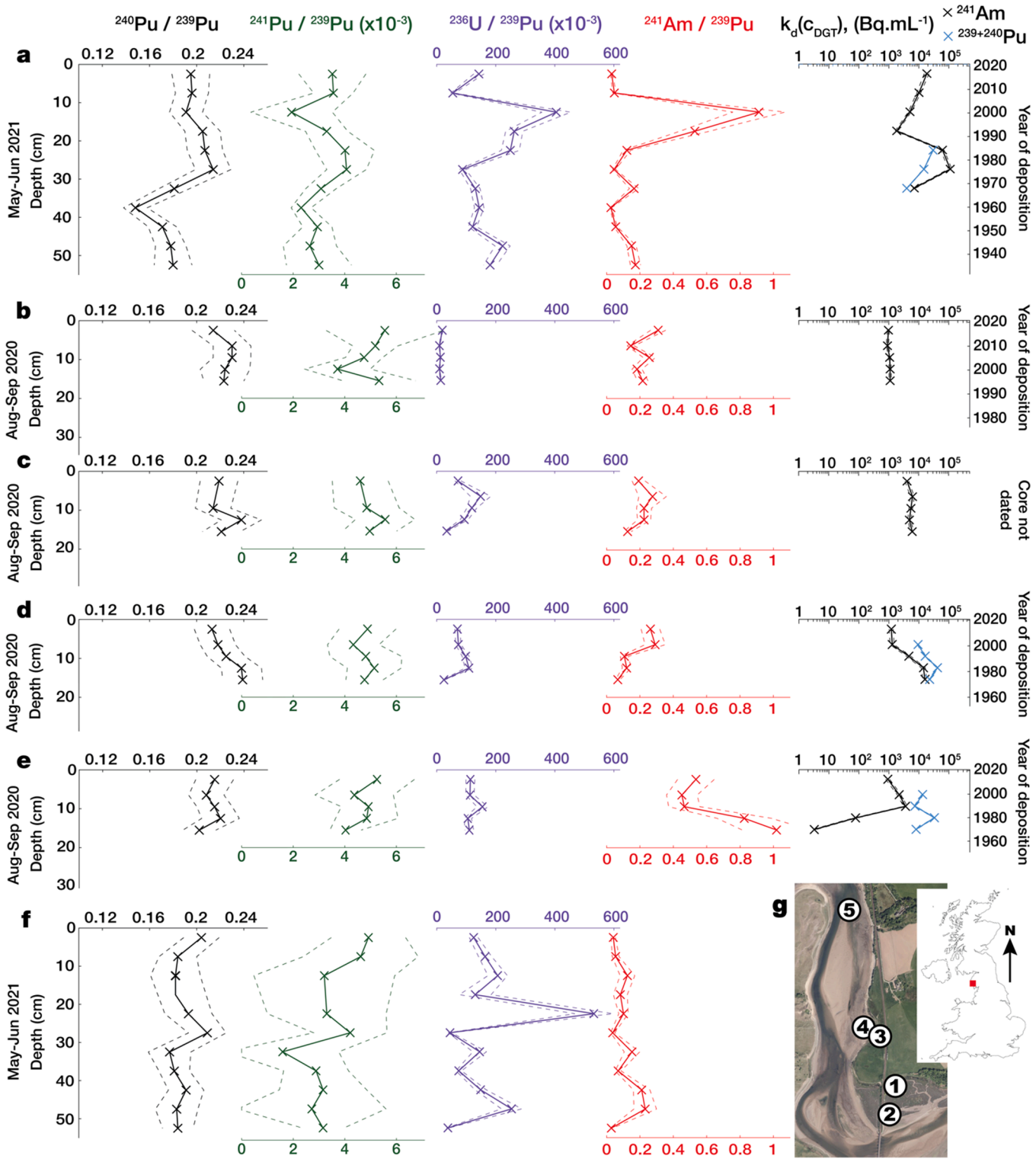

Fig. 2. Isotopic composition and $k_d(c_{DGT})$ throughout the sediment profile at sites 1–5 in the Esk Estuary. Isotopic ratios (atom/atom) according to c_{DGT}, and $k_d(c_{DGT})$ for $^{239+240}$Pu and ^{241}Am at **(a)** Site 1, 24th May–7th June 2021; **(b)** Site 1, 24th August–7th September 2020; **(c)** Site 2, 24th August–7th September 2020; **(d)** Site 3, 24th August–7th September 2020; **(e)** Site 4, 24th August– 7th September 2020; **(f)** Site 5, 24th May–7th June 2021. **(g)** Sampling sites 1–5 in the Esk Estuary. ±2σ uncertainties.

primary purpose of the Sellafield facility was the production of weapons-grade Pu, which requires lower Pu-burn up and therefore has ^{240}Pu/^{239}Pu of <0.07 (Warneke et al., 2002; Ketterer and Szechenyi, 2008)) correlates with a significant drop in the ^{240}Pu/^{239}Pu ratio to 0.148 ± 0.010, indicated by the DGT probe at 35–40 cm depth below Site 1 (Fig. 2a). Ratios remain above 0.14 in these deeper samples however, indicating an attenuation of the weapons-grade signature, either due to remobilisation throughout the sediment column and/ or post-depositional dilution with later sources with higher ^{240}Pu/^{239}Pu, from (and after) the period of peak Sellafield discharges in the 1970s. Furthermore, ^{240}Pu/^{239}Pu ratios at depths corresponding to before the onset of the nuclear age demonstrate remobilisation of Pu downwards

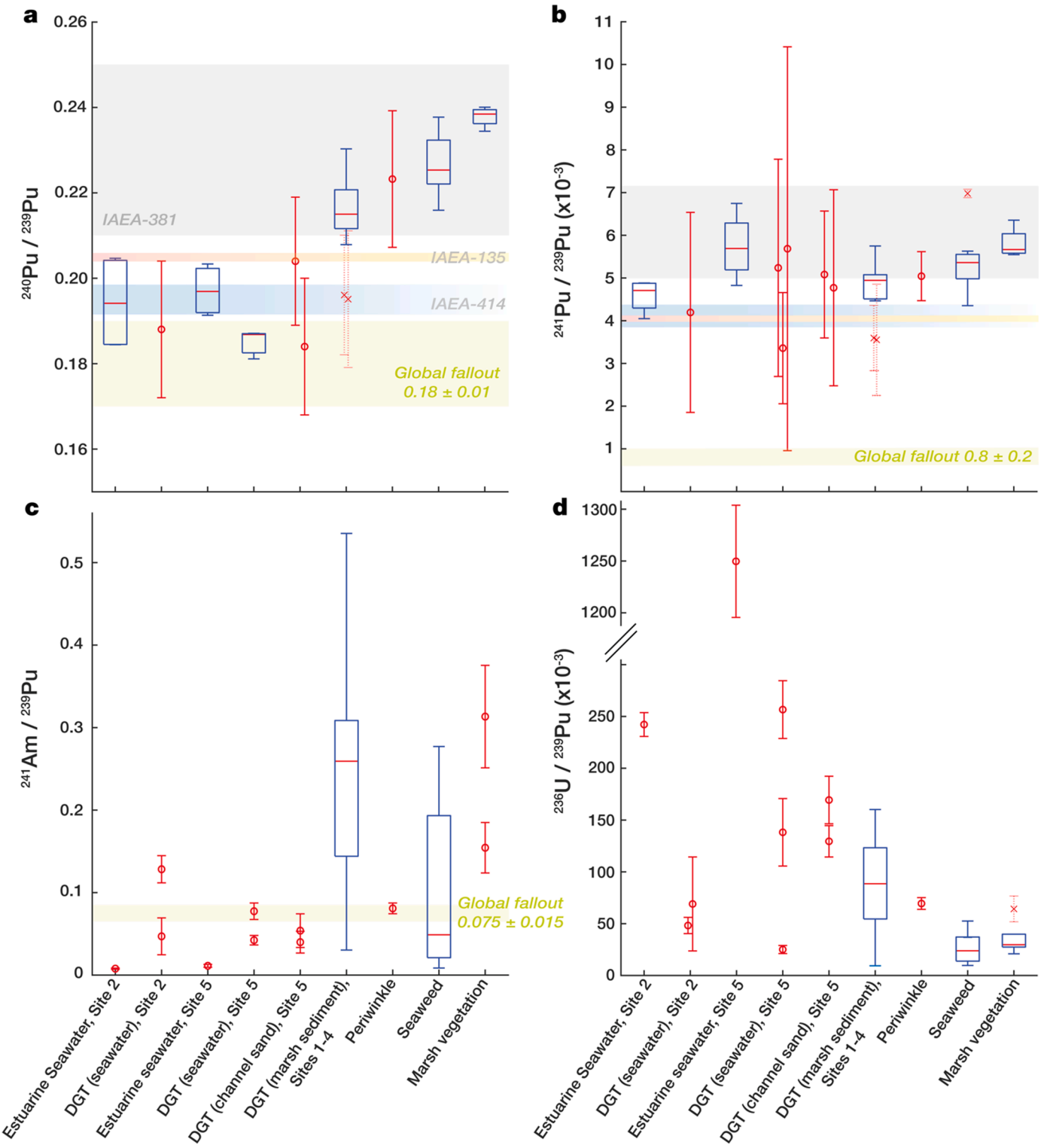

Fig. 3. Isotopic composition of seawater, DGT seawater samplers, DGT sediment samplers and biota in the Esk Estuary. Isotopic ratios (atom/atom) of (**a**) ^{240}Pu/^{239}Pu, (**b**) ^{240}Pu/^{241}Pu, (**c**) ^{241}Am/^{239}Pu and (**d**) ^{236}U/^{239}Pu in (left-right): (1) Bulk seawater (site 2, middle estuary); (2) Seawater DGT samplers (site 2); (3) Bulk seawater (site 5, lower estuary); (4) Seawater DGT samplers (site 5); (5) DGT sampler sections with depth midpoints between 0 and 10 cm at site 5; (6) DGT sampler sections with depth midpoints between 0 and 10 cm at sites 1–4; (7) *Littorina littorae* (soft parts); (8) Internally accumulated fraction of seaweeds (*Fucus vesiculosis* bulk and frond ends, *Chondrus crispus* bulk) and (9) Internally accumulated fraction of marsh vegetation (*Sesuvium porulacastrum, Salicornia Europea and Plantago maritima*). IAEA-135: Irish Sea sediment. IAEA-381: Irish Sea water. IAEA-414: Irish and North Sea fish. IAEA reference values from Corcho Alvarado et al. (2022), ^{241}Pu/^{239}Pu ratios decay-corrected to 15.01.2021 (Supporting Information Table 3). ^{241}Am/^{239}Pu global fallout ratio calculated from the ^{241}Am/$^{239+240}$Pu ratio reported by Froidevaux et al. (2010), assuming global fallout ^{240}Pu/^{239}Pu ratio of 0.18 ± 0.01. Box and whiskers plotted for n ≥ 4. Outliers marked as crosses. ±2σ uncertainties.

throughout the sediment column, through the infiltration of precipitation and/or tidal pumping of seawater in the marsh. This outlines once again the influence of the local hydraulic regime in the remobilisation of Pu in intertidal marshland.

The $^{241}Am/^{239}Pu$ isotopic ratios varied significantly between sites, demonstrating elemental fractionation of the two chemically distinct actinides as a function of the local geochemical conditions. An anomalous peak in the $^{241}Am/^{239}Pu$ ratio to around 1 indicated by the DGT sampler at 10–15 cm below the surface at site 1 (Fig. 2a) likely reflects an increase in k_d for Pu at that depth and/or a decrease in k_d for Am. This correlates with an increase in the c_{DGT} (^{241}Am) and c_{DGT} (^{236}U) concentrations, respectively produced by the separate IIP-Y^{3+}-configured DGT sampler and KMS-1-configured DGT sampler, alongside a decrease in c_{DGT} (Pu) produced by the same KMS-1-configured DGT sampler (Fig. 1a). This effect was not observed nine months previously at the same depth beneath site 1 (Figs. 1b, 2b), pointing to time-specific geochemical conditions that impacted the Pu flux. However, the $^{241}Am/^{239}Pu$ ratio also peaked to around 1 at 14–17 cm below Site 4, but alongside a sharp drop in the $k_d(c_{DGT})$ (the bulk sediment concentration/c_{DGT}) of ^{241}Am (Fig. 2e). The $^{241}Am/^{239}Pu$ ratio is well correlated and inversely proportional to the $k_d(c_{DGT})$ of ^{241}Am at the Brighouse marsh (sites 3 and 4, Fig. 2d, e), but is not closely correlated at the Railway Marsh (Sites 1 and 2, Fig. 2a–c). The sharp drop in k_d is outside of the characteristic range of Am for clays, and better represents that of sands. Finer marsh sediments are known to deposit on top of coarser sand in this area (Clifton and Hamilton, 1982), therefore it is most probable that the lower sections of the DGT sampler were in increasingly coarse sand 11–19 cm beneath Site 4, given its proximity to the sands of the channel. These relationships between the $k_d(c_{DGT})$ and the fluxes demonstrate that k_d is not necessarily the main or sole controlling factor on the remobilisation fluxes of Am, and that a more holistic technique such as DGT is required to assess these.

3.3. Bioaccumulation of actinides from identified sources

We hypothesised that marsh vegetation would accumulate actinides from the root zone (up to 10 cm beneath the surface of the sediments) and thus its isotopic signature should match those of the near-surface sediments, whilst the isotopic signatures of the seaweeds should rather match those of the seawater. In fact, we observed that the higher $^{240}Pu/^{239}Pu$ of the sediments closely matches that of all the biota that we sampled in the estuary (Fig. 3a). This demonstrates the sediments have been the principal supply of Pu to local organisms, indicating the remobilisation of sediment-associated Pu into the local estuarine environment.

The bulk seawater samples from Sites 2 and 5 had a much lower $^{241}Am/^{239}Pu$ signature than the biota (Fig. 3c). There is also a significant difference between the $^{236}U/^{239}Pu$ signatures of the bulk seawater and biota (Fig. 3d). However, the DGT samplers placed *in-situ* for two weeks at the same sites better reflected the $^{241}Am/^{239}Pu$ and $^{236}U/^{239}Pu$ fractionation in the periwinkles, seaweed and marsh vegetation compared to the bulk seawater (Fig. 3c, d). Effectively, DGT more closely reproduced the elemental fractionation in the biota, demonstrating its ability to mimic the diffusive uptake of bioavailable species through living cell membranes and thus provide a bioavailability proxy for Pu, U and Am isotopes.

4. Conclusion

We have demonstrated that DGT presents strong advantages to provide a site-specific and time-weighted appraisal of actinide remobilisation and bioavailability. The variability in the remobilisation fluxes underline the necessity to have an actinide-specific and time-integrated technique at disposition – especially a technique which provides a bioavailability assessment to gauge the radiological impact to organisms. Furthermore, the combination of DGT and AMS allows these data to be produced without requiring the processing of larger and significantly more radioactive samples of sediment and seawater, allowing the assessment of remobilisation fluxes at sub-femtogram levels. We therefore see scope to employ this methodology to improve dose modelling during wider studies of radionuclide remobilisation using DGT. Furthermore, the insights provided here regarding the potential of actinide re-incorporation into the biosphere from sediment will contribute to other environmental projects which must take this into account, such as the near-surface and deep disposal of decommissioning and nuclear reactor/reprocessing wastes.

Authors contributions

J.D.C. developed and manufactured DGT samplers, took part in the planning of field deployments, undertook sampling on-site, performed radiochemical processing of samples, processed and interpreted data, coded and constructed graphics, wrote the manuscript and compiled edits to the manuscript. M.C. performed AMS measurements and data reduction, took part in the planning of field deployments, processed and interpreted data, contributed to the study conception and contributed to the manuscript. A.B.C. and P.E.W. took part in the planning of field deployments, undertook sampling on-site, processed and interpreted data, contributed to the study conception, and contributed to the manuscript. D.G.R. performed gamma spectrometry on sectioned sediment cores, interpreted experimental data and contributed to the manuscript. F.B. supervised and administrated the PhD studentship, took part in the planning of field deployments, interpreted experimental data, contributed to the study conception, and contributed to the manuscript. P.F. conceived the study and the development of DGT samplers, supervised and administrated the PhD studentship, acquired funding, took part in the planning of field deployments, interpreted experimental data and contributed to the manuscript.

Declaration of Competing Interest

The authors declare that they have no known competing financial interests or personal relationships that could have appeared to influence the work reported in this paper.

Data availability

Data will be made available on request.

Acknowledgements

We gratefully acknowledge funding under the Swiss National Science Foundation Grant No. 175492, which supported the PhD studentship associated with this project and the open access publishing of this work. We are also grateful to Jamie, Sam and Tamsin Cundy for their contributions to the on-site fieldwork and to Pawel Gaca for additional laboratory assistance.

Supplementary materials

Supplementary material associated with this article can be found, in the online version, at doi:10.1016/j.watres.2022.118838.

References

Mouri, G., Golosov, V., Shiiba, M., Hori, T., 2014. Assessment of the caesium-137 flux adsorbed to suspended sediment in a reservoir in the contaminated Fukushima region in Japan. Environ. Pollut. https://doi.org/10.1016/j.envpol.2013.12.018.

Taniguchi, K., Onda, Y., Smith, H.G., Blake, W., Yoshimura, K., Yamashiki, Y., Kuramoto, T., Saito, K., 2019. Transport and redistribution of radiocesium in Fukushima fallout through rivers. Environ. Sci. Technol. https://doi.org/10.1021/acs.est.9b02890.

Takata, H., Hasegawa, K., Oikawa, S., Kudo, N., Ikenoue, T., Isono, R.S., Kusakabe, M., 2015. Remobilization of radiocesium on riverine particles in seawater: the contribution of desorption to the export flux to the marine environment. Mar. Chem. 176 https://doi.org/10.1016/j.marchem.2015.07.004.

Cundy, A.B., Croudace, I.W., Warwick, P.E., Oh, J.S., Haslett, S.K., 2002. Accumulation of COGEMA-La hague-derived reprocessing wastes in french salt marsh sediments. Environ. Sci. Technol. 36 (23) https://doi.org/10.1021/es020098c.

Morris, K., Butterworth, J.C., Livens, F.R., 2000. Evidence for the remobilization of sellafield waste radionuclides in an intertidal salt marsh, west Cumbria, U.K. Estuar. Coast. Shelf Sci. 51 (5) https://doi.org/10.1006/ecss.2000.0705.

McDonald, P., i Batlle, J.V., Bousher, A., Whittall, A., Chambers, N., 2001. The availability of plutonium and Americium in Irish sea sediments for re-dissolution. Sci. Total Environ. 267 (1–3), 109–123. https://doi.org/10.1016/S0048-9697(00)00771-3.

Hunt, J., Leonard, K., Hughes, L., 2013. Artificial radionuclides in the Irish sea from sellafield: remobilisation revisited. J. Radiol. Prot. 33 (2), 261. https://doi.org/10.1088/0952-4746/33/2/261.

Mitchell, P.I., Downes, A.B., Vintró, L.L., McMahon, C.A., 2001. Studies of the speciation, colloidal association and remobilisation of plutonium in the marine environment. Radioact. Environ. 1, 175–200. https://doi.org/10.1016/S1569-4860(01)80014-0.

Caborn, J.A., Howard, B.J., Blowers, P., Wright, S.M., 2016. Spatial trends on an ungrazed west cumbrian saltmarsh of surface contamination by selected radionuclides over a 25 year period. J. Environ. Radioact. 151 https://doi.org/10.1016/j.jenvrad.2015.09.011.

Kershaw, P.J., Swift, D.J., Pentreath, R.J., Lovett, M.B., 1983. Plutonium redistribution by biological activity in Irish sea sediments. Nature 306 (5945). https://doi.org/10.1038/306774a0.

Ryan, T.P., Dowdall, A.M., Long, S., Smith, V., Pollard, D., Cunningham, J.D., 1999. Plutonium and Americium in Fish, shellfish and seaweed in the Irish environment and their contribution to dose. J. Environ. Radioact. 44 (2–3), 349–369. https://doi.org/10.1016/S0265-931X(98)00140-4.

Day, J.P., Cross, J.E., 1981. 241Am from the Decay of 241Pu in the Irish Sea. Nature (5818), 292. https://doi.org/10.1038/292043a0.

Agency, I. A. E.*Sediment distribution coefficients and concentration factors for biota in the marine environment*; 2004.

Harper, M.P., Davison, W., Zhang, H., Tych, W., 1998. Kinetics of metal exchange between solids and solutions in sediments and soils interpreted from DGT measured fluxes. Geochim. Cosmochim. Acta 62 (16). https://doi.org/10.1016/S0016-7037(98)00186-0.

Wu, Z., Wang, S., He, M., Wu, F., 2015. The measurement of metals by diffusive gradients in thin films (DGT) at sediment/water interface (SWI) of bay and remobilization assessment. Environ. Earth Sci. 73 (10) https://doi.org/10.1007/s12665-014-3851-z.

Norgbey, E., Li, Y., Ya, Z., Li, R., Nwankwegu, A.S., Takyi-Annan, G.E., Luo, F., Jin, W., Huang, Y., Sarpong, L., 2020. High resolution evidence of iron-phosphorus-sulfur mobility at hypoxic sediment water interface: an insight to phosphorus remobilization using DGT-induced fluxes in sediments model. Sci. Total Environ. 724 https://doi.org/10.1016/j.scitotenv.2020.138204.

Zhang, H., Davison, W., Miller, S., Tych, W., 1995. *In situ* high resolution measurements of fluxes of Ni, Cu, Fe, and Mn and concentrations of Zn and Cd in porewaters by DGT. Geochim. Cosmochim. Acta 59 (20). https://doi.org/10.1016/0016-7037(95)00293-9.

Gao, L., Gao, B., Zhou, H., Xu, D., Wang, Q., Yin, S., 2016. Assessing the remobilization of antimony in sediments by DGT: a case study in a tributary of the three gorges reservoir. Environ. Pollut. 214 https://doi.org/10.1016/j.envpol.2016.04.030.

Zhang, H., Zhao, F.J., Sun, B., Davison, W., Mcgrath, S.P., 2001. A new method to measure effective soil solution concentration predicts copper availability to plants. Environ. Sci. Technol. (12), 35. https://doi.org/10.1021/es000268q.

Davison, W., 2016. Diffusive Gradients in Thin-Films for Environmental Measurements. Editor. Cambridge University Press, Davidson, W., Ed.

Chaplin, J.D., Warwick, P.E., Cundy, A.B., Bochud, F., Froidevaux, P., 2021. Novel DGT configurations for the assessment of bioavailable plutonium, Americium, and uranium in marine and freshwater environments. Anal. Chem. 93 (35), 11937–11945. https://doi.org/10.1021/acs.analchem.1c01342.

Chaplin, J.D., Christl, M., Straub, M., Bochud, F., Froidevaux, P., 2022. Passive sampling tool for actinides in spent nuclear fuel pools. ACS Omega 7 (23), 20053–20058. https://doi.org/10.1021/acsomega.2c01884.

Christl, M., Vockenhuber, C., Kubik, P.W., Wacker, L., Lachner, J., Alfimov, V., Synal, H. A., 2013. The ETH Zurich AMS facilities: performance parameters and reference materials. Nucl. Instrum. Methods Phys. Res. Sect. B Beam Interact. Mater. Atoms 294, 29–38. https://doi.org/10.1016/j.nimb.2012.03.004.

Manos, M.J., Ding, N., Kanatzidis, M.G., 2008. Layered metal sulfides: exceptionally selective agents for radioactive strontium removal. Proc. Natl. Acad. Sci. 105 (10), 3696–3699. https://doi.org/10.1073/pnas.0711528105.

Chauvin, A.S., Bünzli, J.C.G., Bochud, F., Scopelliti, R., Froidevaux, P., 2006. Use of Dipicolinate-based complexes for producing ion-imprinted polystyrene resins for the extraction of yttrium-90 and heavy lanthanide cations. Chem. A Eur. J. 12 (26), 6852–6864. https://doi.org/10.1002/chem.200501370.

Cusnir, R., Steinmann, P., Christl, M., Bochud, F., Froidevaux, P., 2015. Speciation and bioavailability measurements of environmental plutonium using diffusion in thin films. J. Vis. Exp. 105 https://doi.org/10.3791/53188.

Toole, J., Thomson, J., Wilson, T.R.S., Baxter, M.S., 1984. A sampling artefact affecting the uranium content of deep-sea porewaters obtained from cores. Nature 308 (5956). https://doi.org/10.1038/308263a0.

Gray, J., Jones, S.R., Smith, A.D., 1995. Discharges to the environment from the sellafield Site, 1951–1992. J. Radiol. Prot. 15 (2), 99.

Hetherington, J.A., Jefferies, D.F., 1974. The distribution of some fission product radionuclides in sea and estuarine sediments. Neth. J. Sea Res. https://doi.org/10.1016/0077-7579(74)90001-5.

Oh, J.S., Warwick, P.E., Croudace, I.W., 2009. Spatial distribution of 241Am, 137Cs, 238Pu, 239,240Pu and 241Pu over 17 year periods in the Ravenglass saltmarsh, Cumbria, UK. Appl. Radiat. Isot. https://doi.org/10.1016/j.apradiso.2009.02.048.

Marsdem, O.J., Abrahamsen, L., Brayan, N.D., Day Philip, J., Fifield, K., Gent, C., Goodal, P.S., Morris, K., Livens, F.R., 2006. Transport and accumulation of actinide elements in the near-shore environment: field and modelling studies. Sedimentology (1), 53. https://doi.org/10.1111/j.1365-3091.2005.00761.x.

Cusnir, R., Steinmann, P., Bochud, F., Froidevaux, P., 2014. A DGT technique for plutonium bioavailability measurements. Environ. Sci. Technol. 48 (18), 10829–10834. https://doi.org/10.1021/es501149v.

Straub, M., Peña, J., Flury, V., Froidevaux, P., 2022. Uranium stability in a large wetland soil core probed by electron acceptors, carbonate amendments and wet-dry cycling in a long-term lysimeter experiment. Sci. Total Environ. 803 https://doi.org/10.1016/j.scitotenv.2021.149783.

Corcho Alvarado, J.A., Röllin, S., Sahli, H., McGinnity, P., 2022. Isotopic signatures of plutonium and uranium at Bikar atoll, Northern Marshall Islands. J. Environ. Radioact. 242, 106795 https://doi.org/10.1016/j.jenvrad.2021.106795.

McCartney, M., Kershaw, P.J., Allington, D.J., 1990. The behaviour of 210Pb and 226Ra in the Eastern Irish Sea. J. Environ. Radioact. 12 (3) https://doi.org/10.1016/0265-931X(90)90025-Q.

Warneke, T., Croudace, I.W., Warwick, P.E., Taylor, R.N., 2002. A new ground-level fallout record of uranium and plutonium isotopes for northern temperate latitudes. Earth Planet. Sci. Lett. 203 (3–4) https://doi.org/10.1016/S0012-821X(02)00930-5.

Ketterer, M.E., Szechenyi, S.C., 2008. Determination of plutonium and other transuranic elements by inductively coupled plasma mass spectrometry: a historical perspective and new frontiers in the environmental sciences. Spectrochim. Acta Part B Atom. Spectrosc. https://doi.org/10.1016/j.sab.2008.04.018.

Clifton, R.J., Hamilton, E.I., 1982. The application of radioisotopes in the study of estuarine sedimentary processes. Estuarine Coast. Shelf Sci. 14 (4) https://doi.org/10.1016/S0272-7714(82)80013-9.

Froidevaux, P., Steinmann, P., Pourcelot, L., 2010. Long-term and long-range migration of radioactive fallout in a Karst System. Environ. Sci. Technol. https://doi.org/10.1021/es100954h.